INDIAN JOURNAL OF SCIENCE AND TECHNOLOGY

RESEARCH ARTICLE

Assessment of updated low frequency model in delineating bypassed hydrocarbon reservoir: A 4D seismic study of 'X' - field, offshore, Niger Delta, Nigeria

Aniefiok Sylvester Akpan[1]*, **Francisca Nneka Okeke**[1], **Daniel Nnaemeka Obiora**[1]

1 Department of Physics and Astronomy, University of Nigeria, Nsukka, Enugu State, Nigeria

OPEN ACCESS

Received: 01.06.2020

Accepted: 20.06.2020

Published: 07.10.2020

Editor: Dr. Natarajan Gajendran

Citation: Akpan AS, Okeke FN, Obiora DN (2020) Assessment of updated low frequency model in delineating bypassed hydrocarbon reservoir: A 4D seismic study of 'X' - field, offshore, Niger Delta, Nigeria. Indian Journal of Science and Technology 13(36): 3738-3753. https://doi.org/10.17485/IJST/v13i36.770

***Corresponding author**.

aniefiok.akpan.pg79875@unn.edu.ng

Funding: None

Competing Interests: None

Published By Indian Society for Education and Environment (iSee)

ISSN
Print: 0974-6846
Electronic: 0974-5645

Abstract

Aim/objectives: The aim of this research is, to use Time lapse (4D) seismic and investigate the influence of low frequency update in deterministic model-based seismic inversion employed in delineating a prospect saturated with bypassed hydrocarbon accumulation. **Method:** The dataset employed in this study incorporates 4D seismic volumes with fifteen (15) years production, interval between 2001 baseline and 2016 monitor seismic vintages. The inversion was carried out using full bandwidth of the updated low frequency and bandpass filtered low frequency approaches. The seismic vintages (baseline and monitor) were simultaneously inverted into acoustic impedance volumes for the two approaches. The formation fluid and lithology were discriminated through fluid replacement modelling (FRM) based on the colour separation between brine and gas saturation scenarios. **Findings:** The two inversion methods employed reveal six (6) zones suspected to be saturated with bypassed hydrocarbons. The delineated bypassed zones are masked in the full bandwidth approach, depicting the effect of the updated low frequency model. Meanwhile, the bandpass filtered approach result presents a better delineated bypassed reservoir as the zones are more pronounced when compared with the full bandwidth approach. Porosity estimate reveals that the bandpass filtered approach is characterized with excellent porosity in the suspected bypassed zones. The results equally gave more reliable and full delineated bypassed zones. **Originality and novelty:** The dataset employed in this study were obtained from a producing hydrocarbon field which, interest is to maximize the production of oil/gas. The study will bridge the inherent gab observed in using model-based seismic inversion approach to analyse and interpret seismic data in order to delineate hydrocarbon prospects. The research reveals that, the model-based seismic inversion method is still very effective in delineating hydrocarbon prospect when the updated low frequency is bandpass filtered to remove the model effect which influences the inverted acoustic impedance results.

Keywords: Porosity; frequency; bypassed; reservoir and impedance

1 Introduction

The global demand for energy increases yearly with increase in population mostly in the emerging developed nations. Although we have different sources of energy ranging from renewable to non-renewable, oil and natural gas are the most consumed source of energy. Hydrocarbons are expected to remain the major source of energy till at least 2050 as projected by the Annual Energy Outlook [1]. Oil exploration and production companies are faced with the task of increasing this source of energy to meet up with its rate of huge demand, which becomes difficult in recent times. This increasing demand for oil and natural gas has prompted oil/gas exploration and production companies into exploring various measures to enhance the production of oil and natural gas. One of such measures is time-lapse (4D seismic), which involves repeating seismic acquisition over a producing or abandoned oil/gas field in order to monitor production related changes, inefficiencies in the production process and delineates bypassed hydrocarbon accumulation [2–4].

Oil and natural gas are produced from sedimentary rocks which are characterized with faults. The production of this major source of energy causes changes in reservoir parameters, which leaves some volume of hydrocarbon in isolated pockets termed bypassed reservoir. This phenomenon reduces the recovery factor which in-turn hinders the ability of oil exploration and production companies to meet up with the huge demand of oil and natural gas. But, with 4D seismic which involve repeating seismic survey over a field, bypassed hydrocarbon saturated zones are delineated and produced to increase oil/gas recovery. These conditions include; changes in fluid saturation, pressure, temperature, and reservoir heterogeneity over time. As production commences, there is a change in fluid saturation, which causes a corresponding change in pressure that in turn leads to changes in fluid front movement. Another condition which leads to bypassed reservoir is that petroleum is found in regions beneath the earth characterized with faults. Thus, considering the spacing between production wells known to be in kilometres apart, there is a tendency of potential traps being cut-off, thereby impeding the migration of hydrocarbon to the nearby production well. Considering the conventional production technique, it has been observed that we can only produce one-third of the oil in a place [5]. According to [6], the percentage estimation of bypassed oil in sandstone reservoir or deep fans is said to fall between 40 – 80%.

The successes of 4D seismic technique have made oil exploration and production industries not to only concentrate on producing fields but also to look at old offshore and onshore fields with an attempt to delineate bypassed pockets of oil and gas which will lead to increase in hydrocarbon production and maximize return on investment. 4D seismic technique has over the years registered remarkable contributions in enhancing and increasing oil/gas production in known fields across the globe. These include oil/gas fields in USA, North Sea, Europe and West Africa. This paper demonstrates the effect of updated low frequency in delineating bypassed hydrocarbon reservoir in X-field. It emphasizes the need to bandpass filter the updated low frequency to an extent which sizes the seismic bandwidth.

2 Location and Geology of the Study Area

The study area, X–field, is located offshore in Niger Delta (Figure 1 a and Figure 1b), which is a major oil/gas producing sedimentary basin in Nigeria. The basin is situated at the southern end of Nigeria boarding the Atlantic Oceanic and extends from about longitude 3^0E to 8^0E and latitude 4^0N to 6^0N [7,8]. The basin was formed as a result of the build-up sediments associated with rift faulting during the Precambrian [9]. Presently, the basin covers an area of about 75,000 square km and extends from the Calabar Flank and Abakaliki Trough to the Benin Flank, which opens to the Atlantic Ocean in the south. The Tertiary section of the basin is divided into three lithostratigraphic columns: the Benin Formation, Agbada Formation and Akata Formation (Figure 2) by [10]. These formations vary in age of deposition and composition. The Benin Formation overlies the Agbada Formation and comprises the unconsolidated sands and sandstones with thicknesses ranging from 0 to 2100 m [11]. The Agbada Formation underlies the Benin Formation and ranges from Eocene to recent. It consists of alternating sands, silts and shales which are defined by progressive upward changes in grain size and bed thickness [12]. The Akata Formation ranges from Paleocene to recent and comprises of marine shales with sandy and silty beds thought to have been deposited as turbidites. Commercial production of hydrocarbon has been going on in the X-field for the past eighteen (18) years. The field comprises four closely spaced production and exploration wells (Figure 1b). Hydrocarbon in the Niger Delta is produced from sandstones and unconsolidated sands in the Agbada Formation. The reservoirs in the Agbada Formation ranges from Eocene and Pliocene in age which are controlled by depth of burial and depositional environment [13].

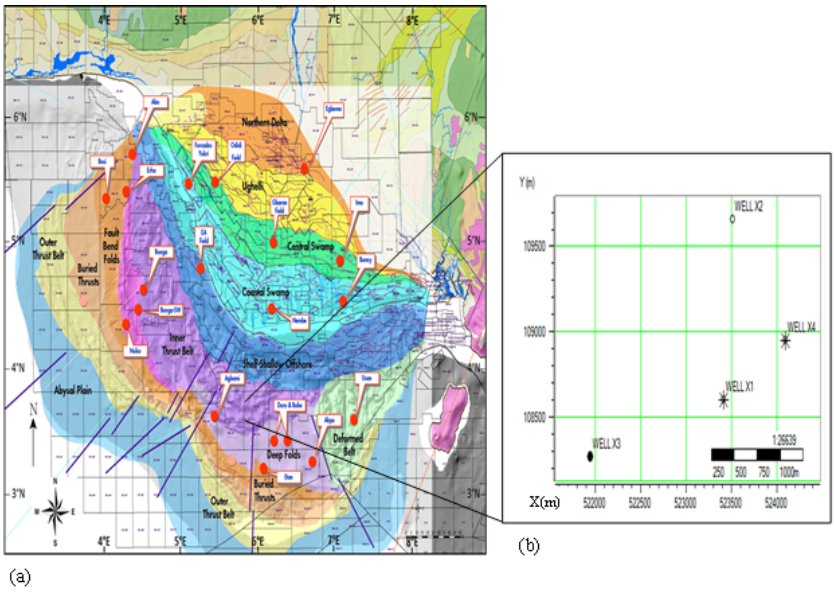

Fig 1. (a) Map of Niger Delta Depobelt showing location of the study area [7] and (b) Base map of X-field showing Seismic Inline/Xline and location of the wells.

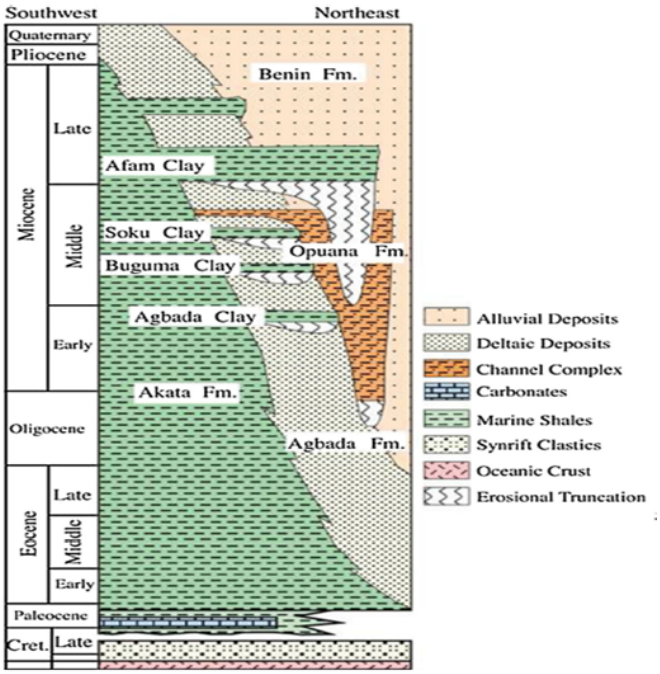

Fig 2. Lithostratigraphic column showing Niger Delta formations [10].

3 Theory of seismic inversion

Seismic inversion is a technique used to transform seismic data into another setting (P-impedance) which results from the product of V_P and ρ [14]. The P-impedance is used to predict lithology and porosity. Seismic inversion provides the most detailed view of the subsurface and because of this efficiency; inversion method is employed by oil and gas companies. Seismic trace occurs as a result of the convolution of Earth's reflectivity with wavelet plus noise [15] given as:

$$S(t) = R(t) * W(t) + N(t) \tag{1}$$

where $S(t)$ is the seismic trace, $R(t)$ is the Earth's reflectivity, $W(t)$ is the wavelet and $N(t)$ is the noise.

Since the noise is removed during processing, the traces in the seismic data are convolution of the earth's reflectivity and a band limited seismic wavelet, expressed by [15] as:

$$S(t) = R(t) * W(t) \tag{2}$$

where, the reflectivity $R(t)$ is related to the acoustic impedance expressed in equation 3 as:

$$R = \frac{v_{k+1}\rho_{k+1} - v_k\rho_k}{v_{k+1}\rho_{k+1} + v_k\rho_k} = \frac{AI_{k+1} - AI_k}{AI_{k+1} + AI_k} \tag{3}$$

where v_k and v_{k+1} are the velocities of the first and second layers and ρ_k and ρ_{k+1} are the densities in the first and second layers respectively.

4 Materials and Method

The data provided comprises well logs from three (3) exploratory wells in the study area. But, due to incomplete log information, the study was carried out using one well labelled well X2 and seismic volumes (baseline and monitor) from a producing X-field acquired at different vintages. The suite of well log which include gamma ray, resistivity, sonic, density and caliper were edited to correct for borehole irregularities encountered during data acquisition. This was achieved by using a median filter with an operator length of six (6) to remove the spikes in the data. Checkshot correction was applied to sonic log to correct discrepancies in the sonic derived P-wave. Two reservoirs sand (HD3000 and HD5000) were delineated using gamma ray and resistivity logs based on high resistivity and low gamma ray curve response. Figure 3 presents the workflow of the study methodology. Reservoir parameters such as; volume of shale, porosity and water saturation were estimated to ascertain the delineated zones as a probable reservoir. S-wave was estimated for the well using [16] relations for sand and shale beds given in equations 4 and 5 respectively.

$$V_S = (0.80416)V_P - 0.85588 \tag{4}$$

$$V_S = (0.76969)V_P - 0.86735 \tag{5}$$

Estimation of the percentage volume of shale present in any reservoir is an important aspect employed in quantifying a zone as probable hydrocarbon bearing reservoir. The shale volume in the delineated reservoirs (HD3000 and HD5000) was estimated using equations 6 and 7 respectively.

$$V_{sh} = 0.083 \times \left(2^{3.7I\ GR} - 1\right) \tag{6}$$

where IGR is the gamma ray index expressed as:

$$IGR = \frac{\left(GR_{\log} - GR_{\text{sma}}\right)}{\left(GR_{\text{shale}} - GR_{\text{smal}}\right)} \tag{7}$$

The terms GR_{log}, GR_{sand}, and GR_{shale} are the gamma ray (GR) Values in API units. The sand (GR_{sand}) and shale (GR_{shale}) baseline are the minimum and maximum values, respectively, in the gamma ray log.

Porosity (ϕ) defined by [17] is the volume of pores or void spaces found in a rock, which determine the rock's capacity to store or transmits fluids. This reservoir parameter was estimated from density log using equation 8 by [18] given as:

$$\phi = \frac{\rho_{ma} - \rho_b}{\rho_{ma} - \rho_f} \tag{8}$$

ρ_b is the bulk density of the formation, ρ_{ma} is the density of the rock matrix and ρ_f is the density of the fluids occupying the pore spaces.

Resistivity log which serves as major fluid indicator tool was employed in estimating the formation water saturation using equation 9 given by [19] as;

$$S_W^n = \frac{a}{\phi^m} \times \frac{R_W}{R_t} \tag{9}$$

where; a, is the cementation factor, m is the cementation exponent, R_w is resistivity of the formation water, and n is the saturation exponent.

Fluid substitution modelling was carried out for varying fluid saturations. Gas and brine were varied using 50% saturations for each case scenario. The 4D seismic quality control (QC) was carried out using crosscorrelation. The crosscorrelation slice (Figure 4) depicts a maximum correlation of 0.94 and minimum of 0.75 percent, which indicate good correlation between the seismic vintages. Statistical wavelet was extracted (Figure 5) from the baseline and tied to the well after which a final wavelet with updated low frequency model was extracted using well option (Figure 6). Horizons (1 & 2) corresponding to the delineated reservoirs (HD3000 & HD5000) were picked across the seismic super volume.

Acoustic impedance model was established from the baseline volume using full bandwidth of final wavelet with updated low frequency (Figure 7). The 4D seismic vintages were simultaneously inverted into acoustic impedance using [20] simultaneous inversion approach. This was done using the full bandwidth of the updated low frequency and bandpass low frequency approach. In the bandpass approach, frequency cut-offs which sizes the seismic bandwidth were defined for low pass (LP), high pass (HP), high cut (HC) and low cut (LC) as shown in Figure 8 . LC is the minimum frequency below which no signal is retained while low frequencies are gradually admitted up to the value provided by LP. HC is the signal maximum frequency where no noise is retained above it and LP is the frequency at which the signal starts to be removed. The [20] simultaneous inversion workflow adopted for the 4D seismic inversion is shown in Figure 9 . The model inverted acoustic impedance was used to generate P-impedance attribute and amplitude slices from the inverted baseline and monitor volume. The P-impedance amplitude slices were differenced and possible bypassed reservoirs inferred in the study area. Also, effective porosity across the suspected bypassed reservoirs was estimated from the difference amplitude slices for the approach – full bandwidth and bandpass.

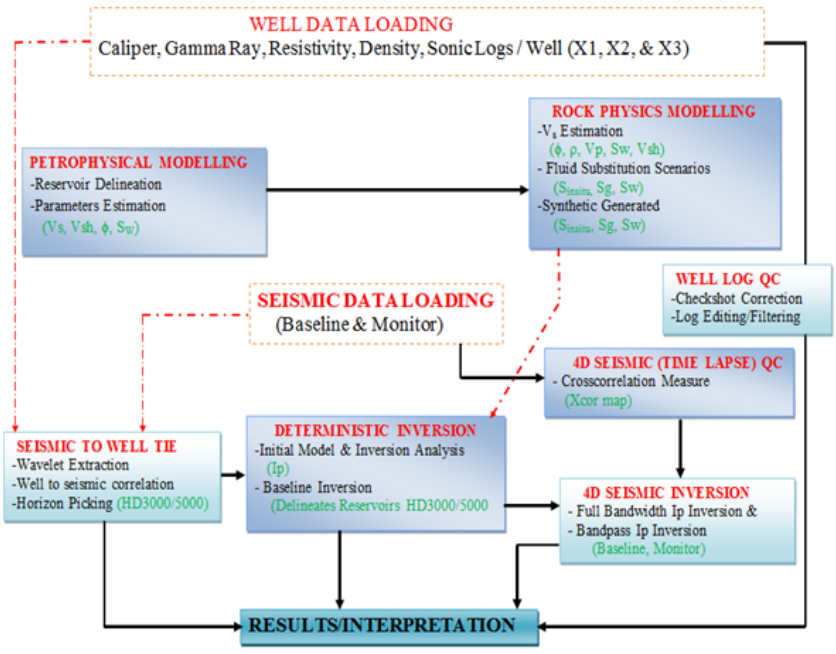

Fig 3. Summarized work flow illustrating the study methodology.

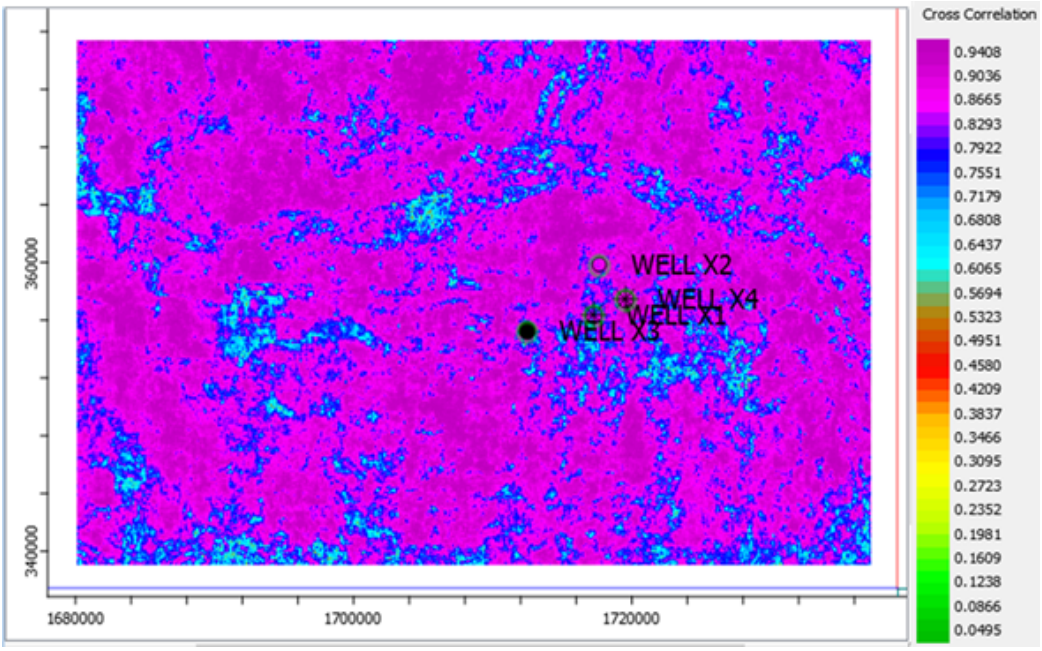

Fig 4. Crosscorrelation slice showing the correlation percentage of the baseline and monitor

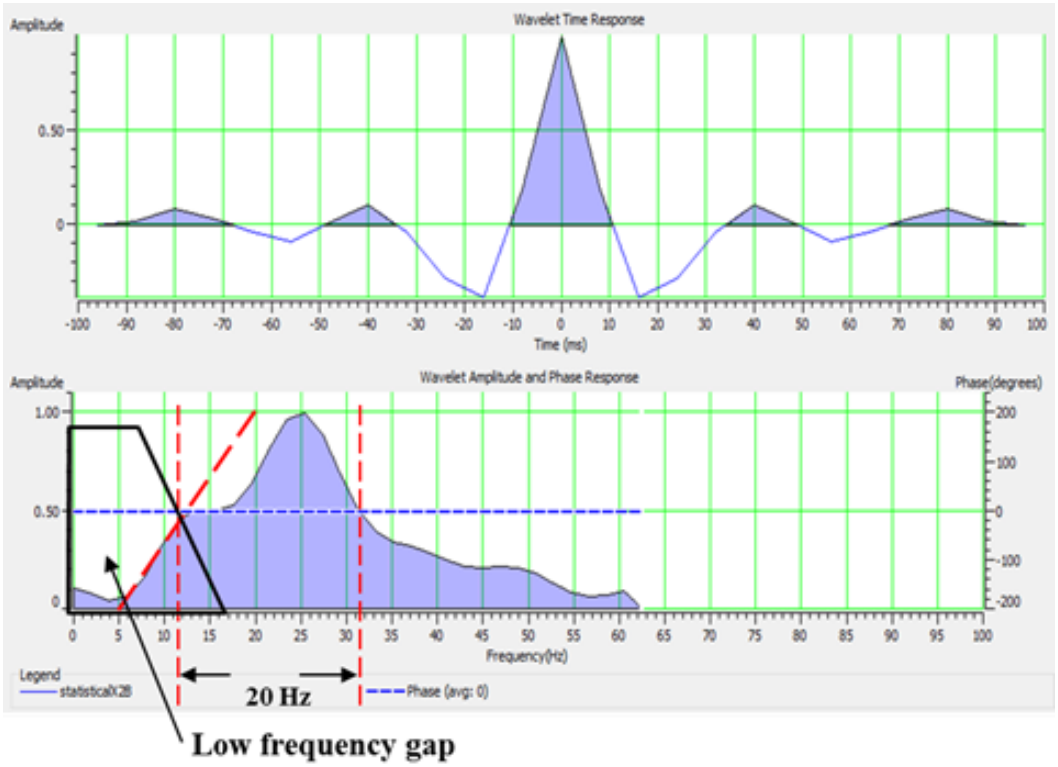

Fig 5. Statistical wavelet extracted around well X2 showing the time and frequency response respectively with the loss of low frequency below 10 Hz.

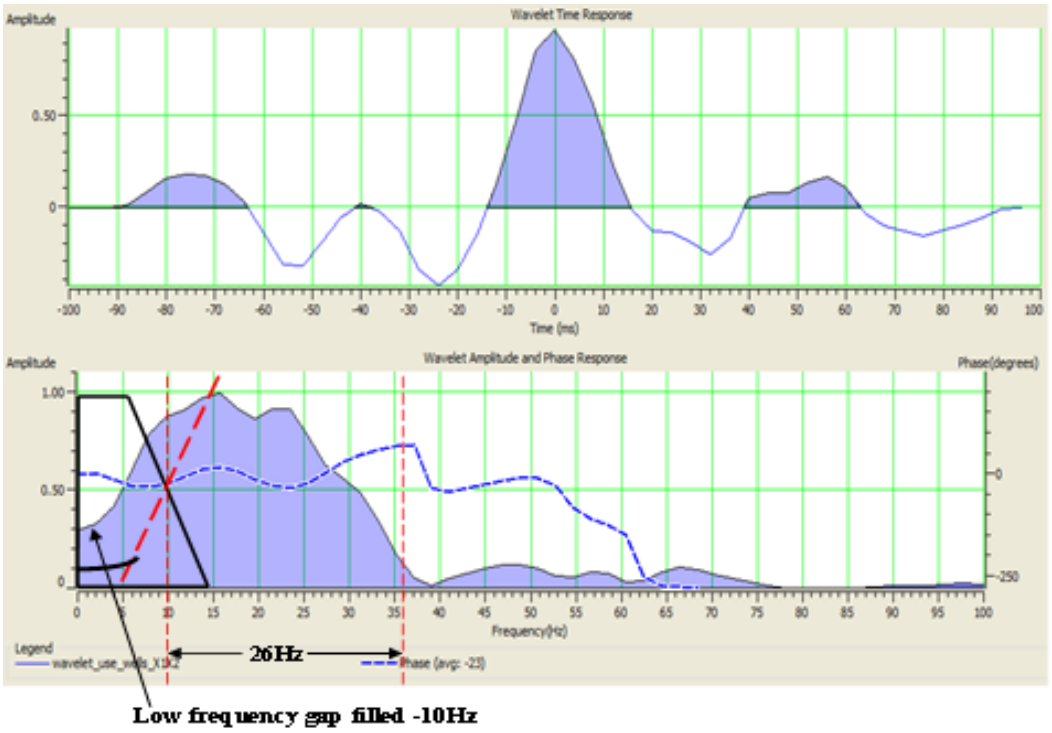

Fig 6. Final wavelet extracted with updated low frequency showing the time and low frequency response respectively with 10 Hz low frequency gap filled.

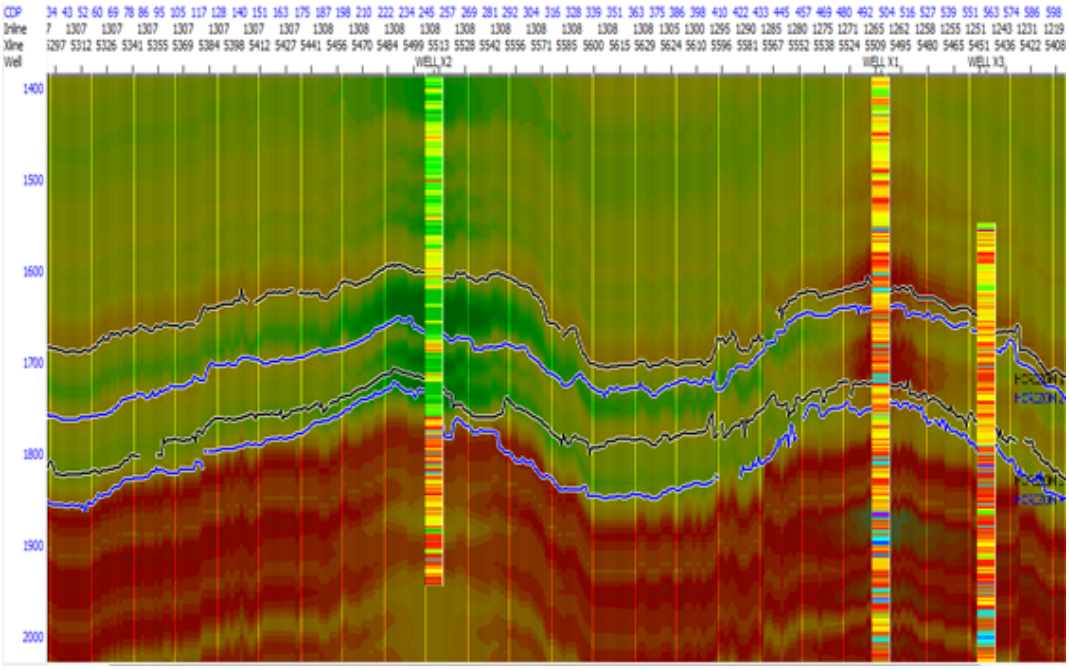

Fig 7. Acoustic impedance initial model section showing P – impedance log plots of the wells in the field.

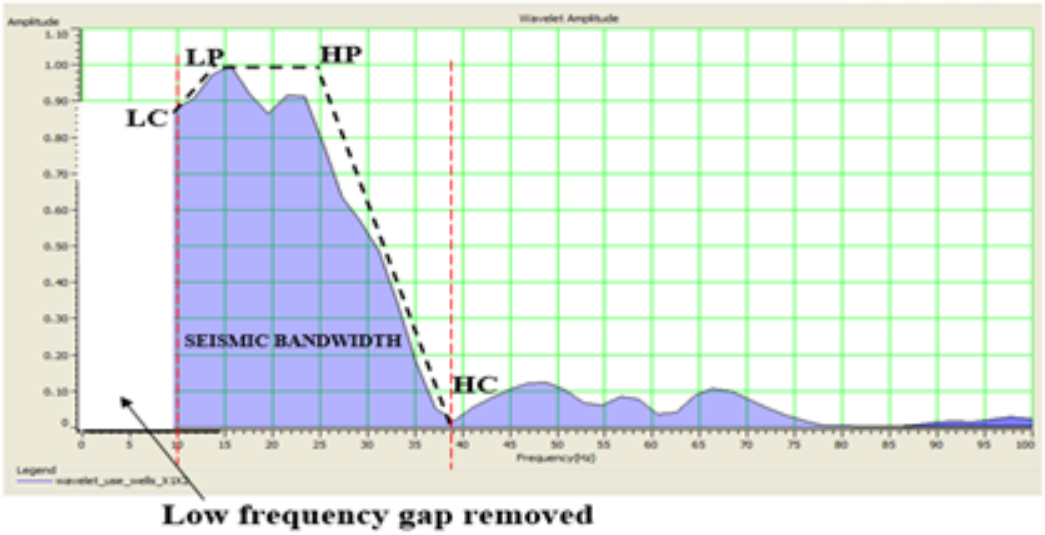

Fig 8. Bandpass filtered wavelet from the updated low frequency wavelet.

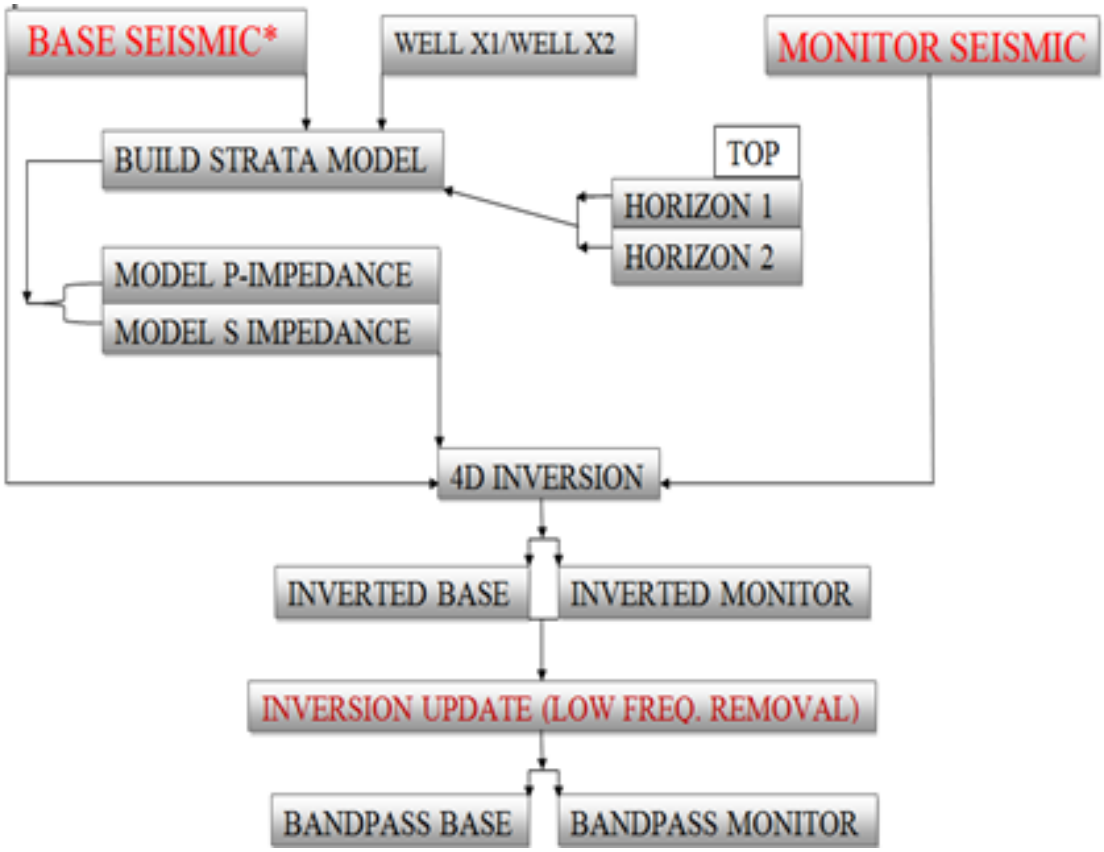

Fig 9. The 4D seismic inversion work flow of the study.

5 Results and discussion

5.1 Results of well log interpretation and estimated reservoir parameters

The results of well log interpretations and estimated reservoir parameters of well X2 are shown in Figure 10 a and b. The wells exhibit dominantly sand, sand/shale and shale lithologic succession, which are attributed to the formations in the Niger Delta Basin. Sand lithology is characterized by low gamma response (<60 API) while shale lithology is characterized with high gamma response (>60 API) values in track 1. Reservoir parameters estimated include; porosity (ϕ), volume of shale (V_s), and water saturation (S_W). These reservoir parameter values are within the industry standard for potential reservoir (sand lithology) saturated with hydrocarbon. Within the reservoir zones (HD3000 and HD5000) circled with black, resistivity is high with the highest kick close to 2000 Ωm in HD3000, which is suspected to be due to the presence of gas as pointed out by [21].

The reservoir zones have excellent effective porosity (>30 %) when compared to the standard porosity values given by [22]. Volume of shale (V_S) result is high outside the reservoir zones and low within the reservoirs (<25%). Within the reservoirs, shale volume increases in region with intercalated sand/shale and shale intruded region. Water saturation is less than 10% in the reservoir but increases at the bottom of HD5000 as a result of shale intrusion as indicated in the gamma ray log signature. Also, resistivity log maintains a steady decrease towards the bottom of HD5000 reservoir. This region is characterized with shale intrusion by the gamma ray curve. The delineated reservoirs (HD3000 and HD5000) are characterized with low water saturation, excellent effective porosity, high resistivity, low volume of shale and low gamma ray values. These reservoirs are active hydrocarbon reserves in the study area with reservoir properties that can accumulate extractable amount of hydrocarbon in the field. The reservoirs range from 6144 to 6245 ft and 6450 to 6540 ft for HD3000 and HD5000 respectively. These ranges of values give a reservoir thickness of 101 ft and 90 ft.

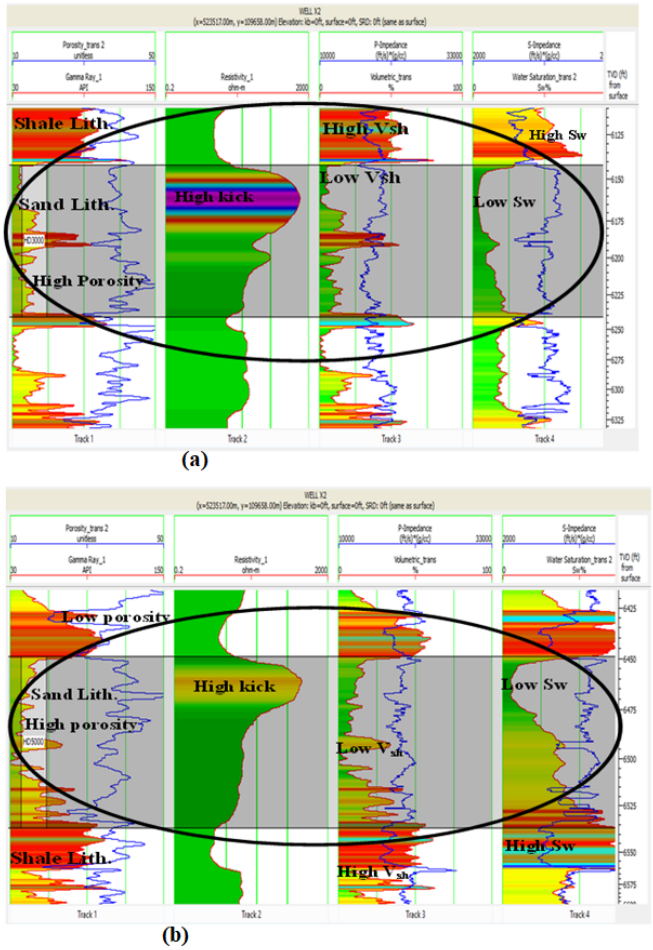

Fig 10. Delineated HD3000 and HD5000 sand reservoirs and estimated reservoir parameters (a) HD3000 and (b) HD5000.

5.2 Fluid substitution modelling results

The results of the fluid substitution for the cases – gas and brine saturations are shown in Figure 11 a and b. The injection of 50% gas into the reservoirs causes the in-situ (red curve) P-wave to decrease from 8263.10 ft/s to 7223.90 ft/s (blue curve) in HD3000 while in the HD5000; the decrease is from 9636.35 ft/s to 9198.36 ft/s (Figure 11a). The variation in density is such that, density decreases more with 50% gas injection compared to the second case where brine was injected into gas saturated model. In-situ density decreased from 2.07 g/cc to 1.70 g/cc in HD3000 and 2.11 g/cc to 1.77 g/cc in HD5000. The result of the second

case is shown in Figure 11 b and In HD3000, the in-situ (red curve) P-wave decreases from 8263.10 ft/s to 7995.52 ft/s and in HD5000 the decrease is from 9636.35 ft/s to 9019.70 ft/s (Figure 11b). For this case scenario, density variation with brine injection depicts high increase in the reservoir when compared with the in-situ. The in-situ density increased from 2.07 g/cc to 2.80 g/cc in HD3000 while in HD5000 the increase from in-situ is 2.11 g/cc to 2.80 g/cc. The different changes observed in P-wave and density in the two reservoirs HD3000 and HD5000 confirms the effect of different fluid saturations on seismic waves.

The synthetic scenario model for gas and brine substitution is such that; at the top of the reservoirs, the gas and brine saturation cause changes in the colours and the generated synthetic traces, which indicate the presence of each fluid injected. For the gas injection, the response of the synthetic traces is such that amplitude increases negatively when compared to the in-situ model. With the injection of 50% gas into the reservoir, the tops of the two reservoirs, HD3000 and HD5000 are completely filled with green colour indicating low impedance sand which is usually attributed to hydrocarbon saturated rock. An entirely opposite response is observed in the case where the reservoirs are substituted with 50% brine. Amplitudes of the generated synthetic traces increase positive and tops of the reservoirs HD3000 and HD5000 are filled with purple colour. These model results and the synthetic scenarios ascertain the relationship between each formation fluid and the expected colour response, which served as constraint in delineating the probable bypassed reservoirs in the study area. From the results, hydrocarbon charged sands have been clearly distinguished from background shale/water sand using the colour separations. As stated by[23], a standard way of relating P-wave seismic velocity to changes in fluid saturation is to use the Gassmann's model.

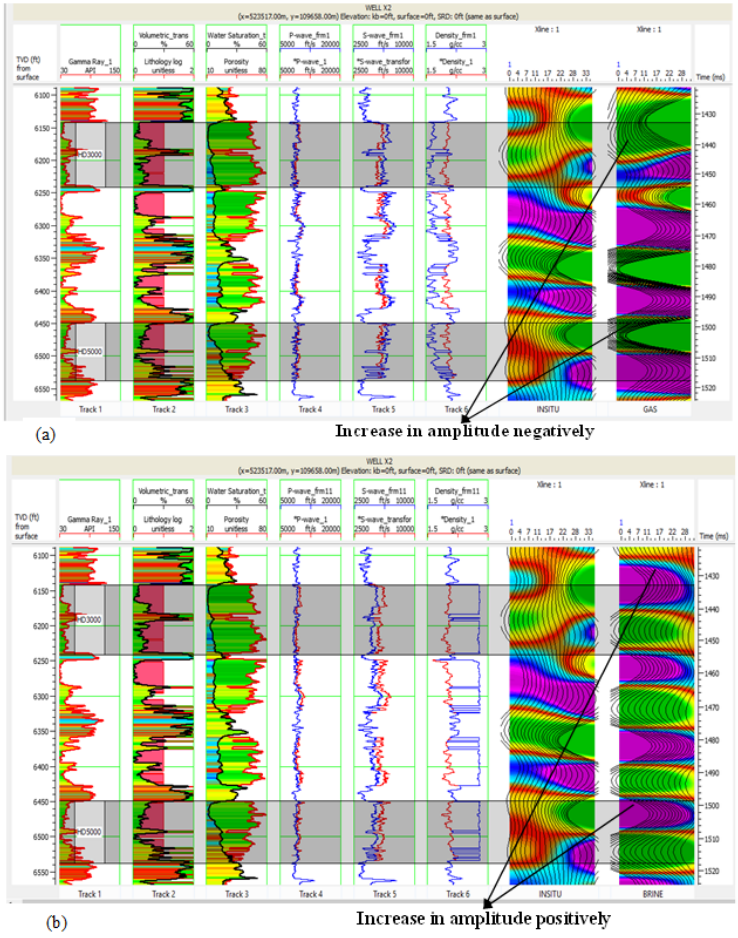

Fig 11. Fluid substitution modeling result showing thein-situ and generated synthetic traces (a) Gas (b) Brine.

5.3 4D Simultaneous inversion results for updated and bandpass low frequency model

The 4D simultaneous inverted P-impedance results cross sections of the baseline and monitor volumes for the selected target window of 1400 to 2000 ms obtained using the updated low frequency wavelet are shown in Figure 12 a and b. The results depict the use of model based technique in generating quantitative estimates of the baseline and monitor seismic volumes which is common input in reservoir modelling. The match between the inserted Ip curve of the three wells and the inverted baseline and monitor volumes depicts a fair distribution with the Ip features. The area marked in rectangle shows the influence of the updated low frequency (full bandwidth) in the inverted baseline and monitor. The effect is clearly seen around well X2 where gas was injected into the reservoir meanwhile no influence is observed around wells X1 and X3. The sections depict moderate changes between the baseline and monitor volume with reservoir sands that are not readily identified away from the injected gas zone. The highest Ip values are observed in blue and purple, and correspond to shale beds ranging from $2.07 - 2.22 \times 10^4$ ft/s*g/cc. The intermediate Ip in red and cyan with values ranging from $1.87 - 2.05 \times 10^4$ ft/s*g/cc are the brine saturated sands. The lowest Ip features are observed in green and yellow with values ranging from $1.67 - 1.85 \times 10^4$ ft/s*g/cc is the hydrocarbon charged sands. The full

bandwidth 4D difference volume of the inverted baseline and monitor is shown in Figure 13. The results reflect 4D effects across the reservoir areas, which extend to well X1 and X3 where brine saturated sands are replaced with hydrocarbon charged sands due to production.

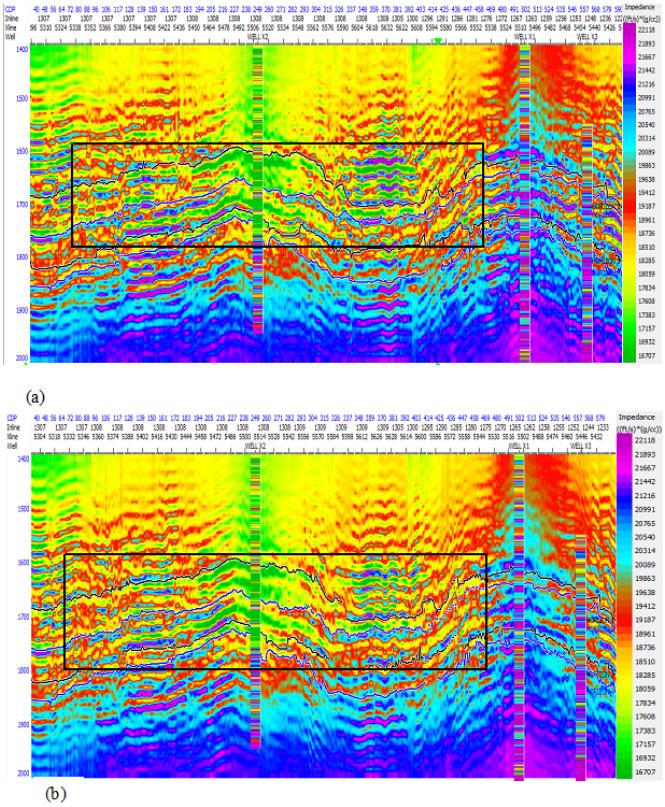

Fig 12. Full bandwidth simultaneous inverted P-impedance volume from time window of 1400 – 2000 ms (a) baseline and (b) monitor.

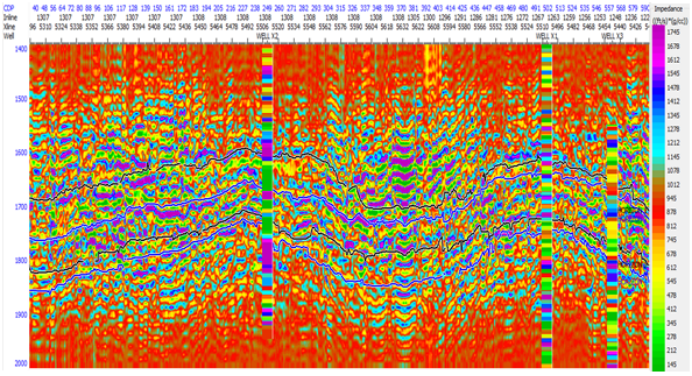

Fig 13. Simultaneous inverted P-impedance difference volume (baseline – monitor) from a time window of 1400-2000 ms for the full bandwidth updated low frequency.

5.4 Bandpass low frequency (filtered) 4D inversion results

The bandpass filtered low frequency inversion results for the baseline and monitor volume shown in Figure 14 a and b, produced a more detailed P-impedance section than the inverted results obtained using full bandwidth of the updated low frequency. The inverted volume cross sections, which run from a time window of 1400 to 2000 ms exhibits a good match between the Ip features of the inverted seismic volume and the inserted wells. The bandpass filtering method enhances the seismic contribution and increases the signal to noise ratio with absolute changes in the Ip results. The rectangular area incorporates the two reservoir sections showing the continuity of the delineated reservoirs away from well X2. Reservoir sands saturated with hydrocarbon are readily identified as the updated low frequency is filtered from the wavelet using the bandpass cut-offs. The highest Ip values within the area correspond to shale beds ranges

from $1.32 - 1.74 \times 10^3$ ft/s*g/cc in blue and purple colours. The lowest Ip values which is observed are the hydrocarbon charged sands with Ip values ranging from $1.58 - 5.68 \times 10^2$ ft/s*g/cc in green and yellow colours. Figure 15 shows the inverted 4D difference volume of the baseline and monitor indicating well pronounced 4D effects across the volume.

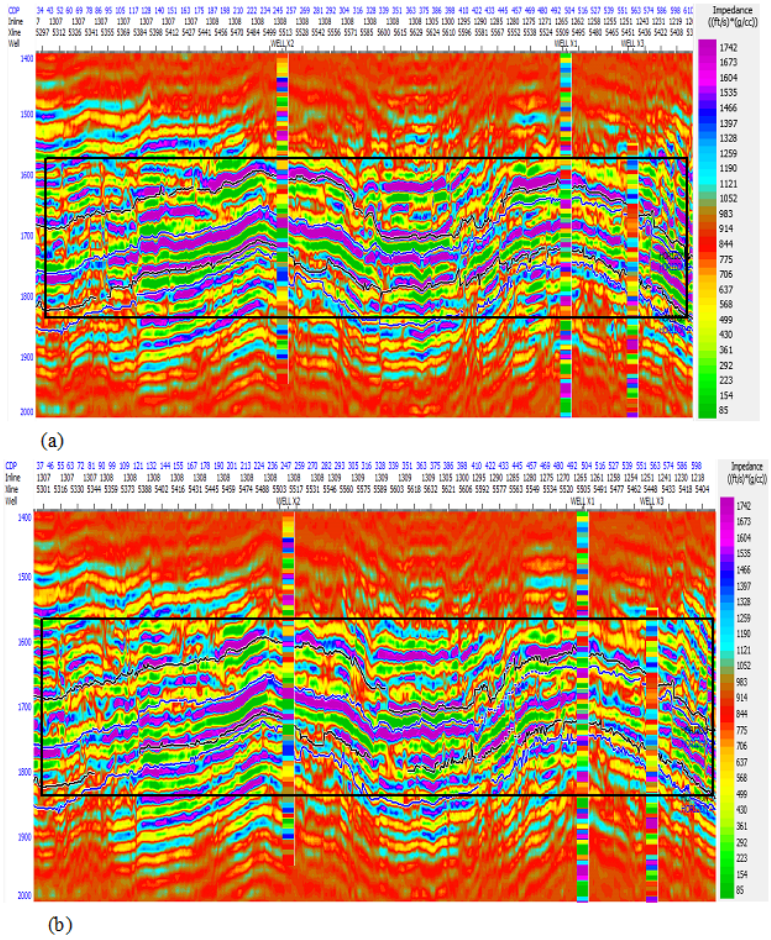

Fig 14. Bandpass low frequency simultaneous inverted volume from a time window of 1400-2000 ms (a) baseline and (b) monitor.

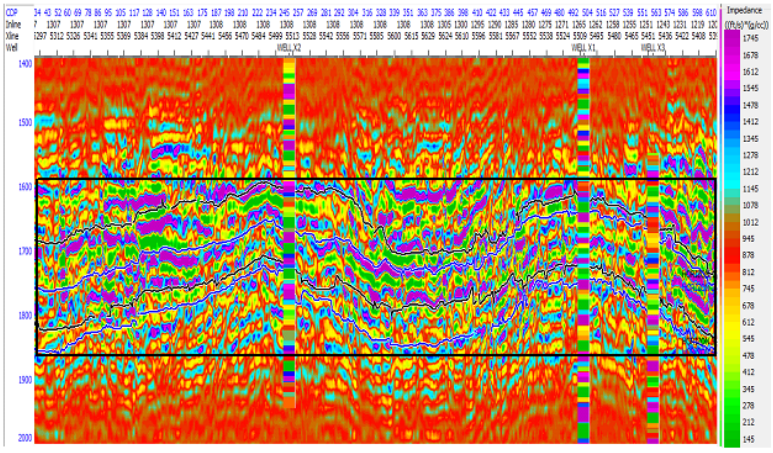

Fig 15. Simultaneous inverted P-impedance difference volume (baseline – monitor) from a time window of 1400 – 2000 ms for thebandpass low frequency.

5.5 P-impedance amplitude (Zp) slice map results

The impedance amplitude slice results from the inverted baseline and monitor are shown in Figure 16 (a and b) and Figure 17 (a and b) for the full bandwidth and bandpass inverted P-impedance sections. These results depict 4D effects which occur as a result of hydrocarbon production from the field over time. This is evident in the acoustic impedance values across the well locations in which the monitor amplitude increases over the baseline impedance amplitude. Figure 17 (a and b) represent the amplitude slices from the full bandwidth and this reveals the influence of low frequency supplied in model-based inversion method. From the results, hydrocarbon accumulation in the baseline and possible depletion is observed in the monitor amplitude slice as being less in other areas of the field when compared to the saturation around well X2. The prospective hydrocarbon saturation, which exists around well X2 with changes in impedance, is due to the low frequency from the injection of gas in the model. The impedance response around well X2 validates this proof; as the area seems to be saturated with much hydrocarbon accumulation, which is reverse when the low frequency is filtered out using the bandpass method. The result indicates that only well X2 is saturated with hydrocarbon while well X1 is completely flushed out and replaced with brine.

Figure 17 (a and b) represent the impedance amplitude (Zp) slice map for the bandpass method where filtering was employed to remove the user supplied low frequency effect from the baseline and monitor. The 4D effect between the baseline and monitor slices are clearly evident in this case as shown in areas marked with circle in the monitor Zp slice. It reveals changes in saturation and watered out areas characterized with increase or decrease in Zp depending on the changing fluid type; that is either oil replacing water or water replacing oil. Well X1, which was producing in the baseline during the onset of production is completely swept in the monitor Zp slice. Also, well X2 is still producing as seen in the monitor Zp slice but has low hydrocarbon accumulation when compared to what was observed in the inversion result of the full bandwidth. This clearly ascertains the influence of low frequency in the conventional deterministic model-based inversion approach as seismic interpreters end up interpreting more of the model result than the seismic contribution. From the monitor Zp, brine is gradually encroaching into the hydrocarbon saturated areas as seen in the Zp values increasing in some of the areas. This is also evident in the Zp values around the wells in the monitor when compared to the baseline slice. From [24], the increase in P-impedance is said to occur as a result of; water replacing hydrocarbon fluids, oil replacing gas, and decline in reservoir pressure or porosity loss as a result of compaction. The entire monitor amplitude slice depicts washout effects across the area indicating reduction in hydrocarbon saturation as at when the monitor data was acquired.

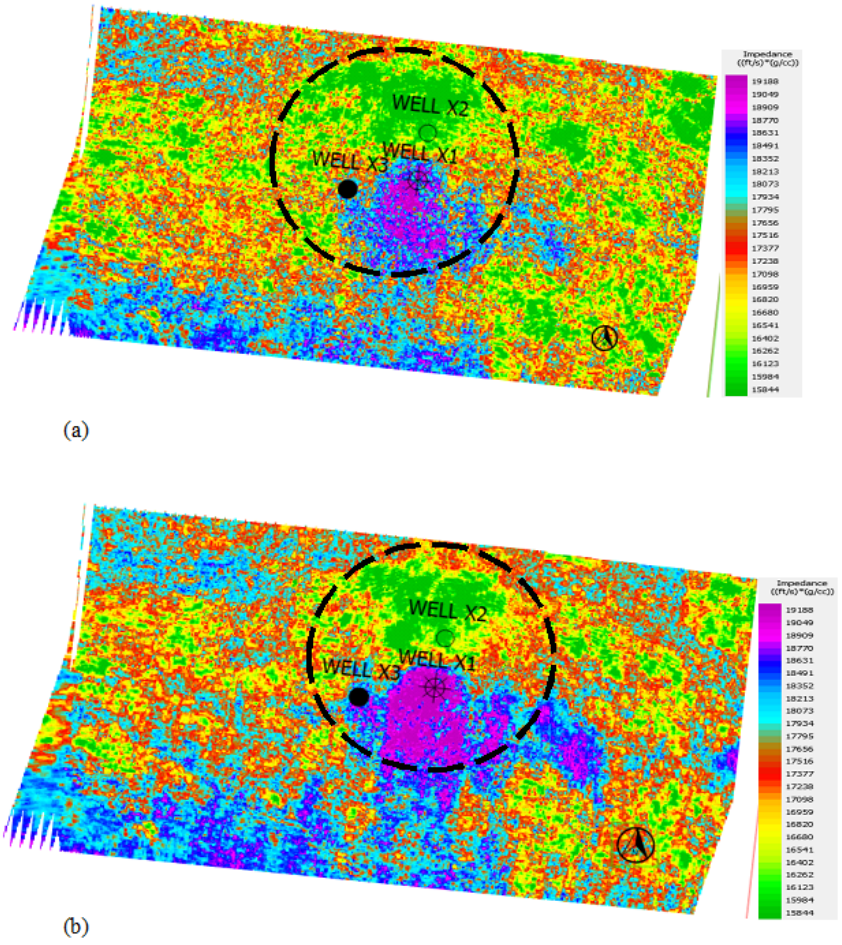

Fig 16. Amplitude slice (Zp) of the horizon from the full bandwidth 4D inverted P-impedance (a) baseline and (b) monitor.

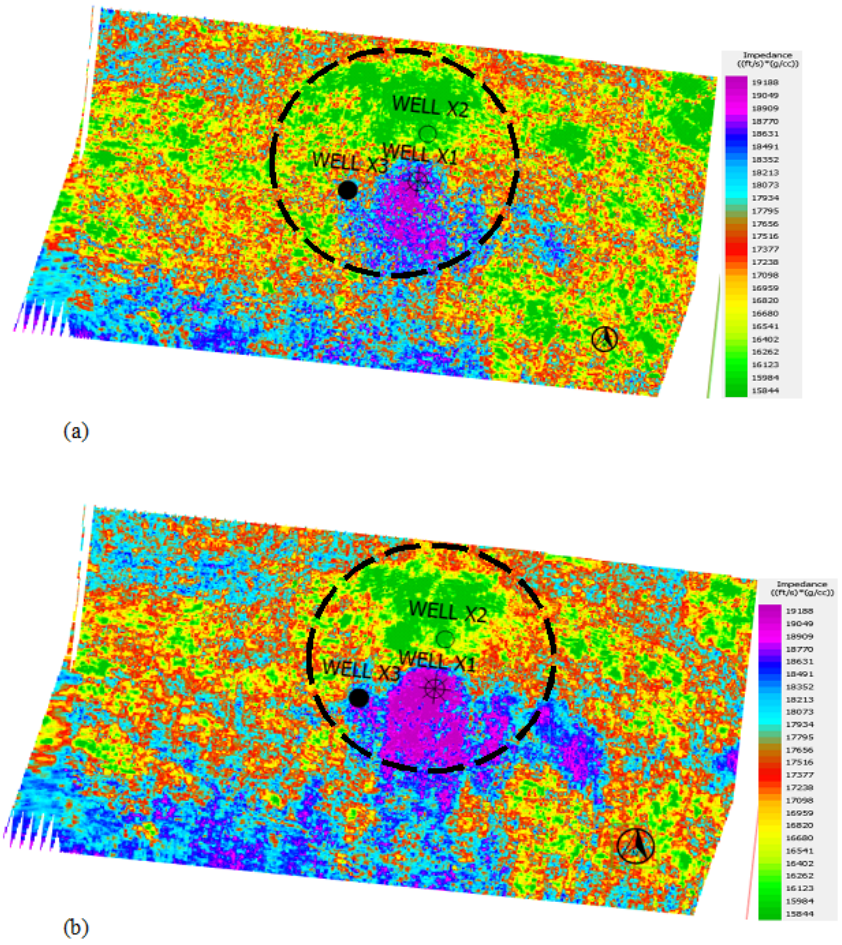

Fig 17. Amplitude slice (Zp) of the horizon from theband pass filtered 4D inverted P-impedance (a) baseline and (b) monitor.

5.6 P-impedance amplitude difference map results for full bandwidth and bandpass

The amplitude difference map which reveals areas with bypassed reservoirs are shown in Figure 18 (a and b) and Figure 19 (a and b) for the full bandwidth and bandpass approach respectively. The difference in map distribution over time allows easy identification of undrained hydrocarbon sands. From the results, six (6) zones, which are reservoirs saturated with bypassed hydrocarbons are delineated. The differences in impedance between the inverted baseline and monitor minimize the effects of lithologic variations on elastic properties and emphasize the effects of production [24]. The problem with updated low frequency in impedance inversion results is clearly seen when the results of the two approaches are considered as shown in their respective amplitude difference slices. The undrained zones with potential hydrocarbon prospects are masked in the full bandwidth approach (Figure 18a) which is due to the low frequency supplied in the model building. The region around well X2 in Figure 19 a shows that well X2 is still producing in line with the monitor amplitude (Zp), which revealed some appreciable hydrocarbon accumulation. The region marked purple to cyan with increase in impedance values when compared to the baseline amplitude is as a result of water replacing oil/gas. This observation is consistent with the Gassmann fluid substitution modelling where brine substitution was characterized with positive increase in the generated synthetic traces.

The estimated effective porosity of the delineated undrained zones is shown in Figure 18 b and Figure 19 b. The porosity attribute, which is one of the properties used in quantifying a reservoir, describes the flow model of the delineated bypassed reservoirs. It reveals excellent connectivity within the zones delineated with bypassed hydrocarbon reservoirs. From the results, the bypassed hydrocarbon zones for the bandpass filtered approach have high porosity values, which agree with industry values for excellent connectivity in an oil/gas reservoir. Alternatively, the porosity estimated for the full bandwidth delineated bypassed zones reveals low porosity when compared to the bandpass approach, which further validates the influence of updated low frequency in model-based inversion analysis approach. The interpretation of porosity as well as fluid contents from acoustic impedance has contributed immensely to limiting exploration risks and hydrocarbon resource evaluation in challenging reservoirs [25–27]. The Zp and effective porosity values indicate that the delineated zones are high productive areas saturated with yet to drilled prospects in the field. These undrained zones were mapped based on the level of water saturation in purple colour, which represent brine in Gassmann fluid modelling scenario and green colour with low acoustic impedance values for hydrocarbon saturated beds. As [21] points out, low P-impedance values denotes a sand lithologic units with high porosity and hydrocarbon saturation. The full bandwidth porosity estimate reveals that model based Zp with supplied low frequency is not best suited for estimating effective porosity as the low P-impedance to low porosity transformation relation implies error in tracking the bypassed oil/gas zones.

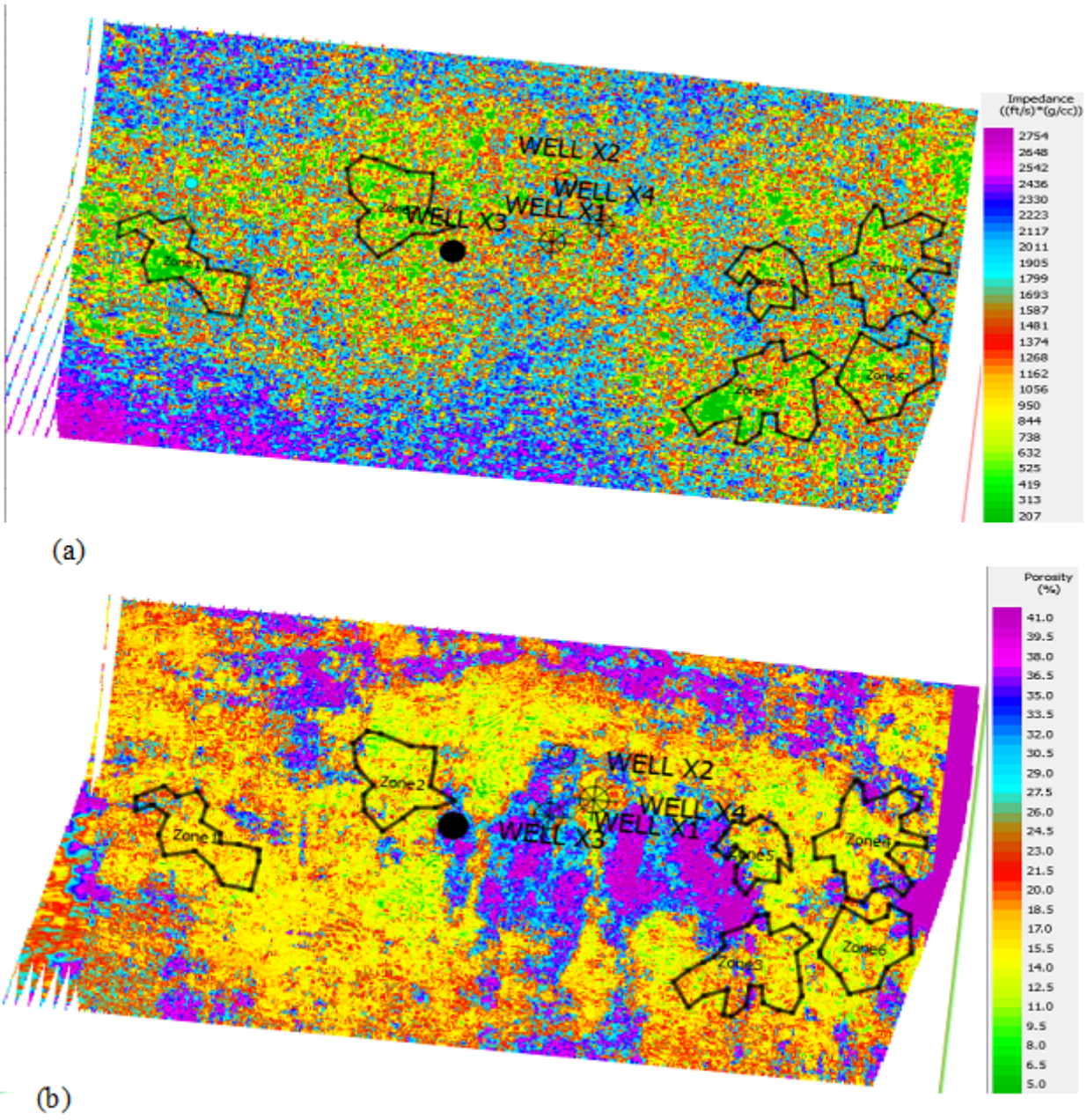

Fig 18. a. Amplitude (Zp) difference map of the fullbandwidth showing delineated bypassed zones.
b. Porosity estimation slice for full bandwidthshowing low around the delineated bypassed reservoir zones.

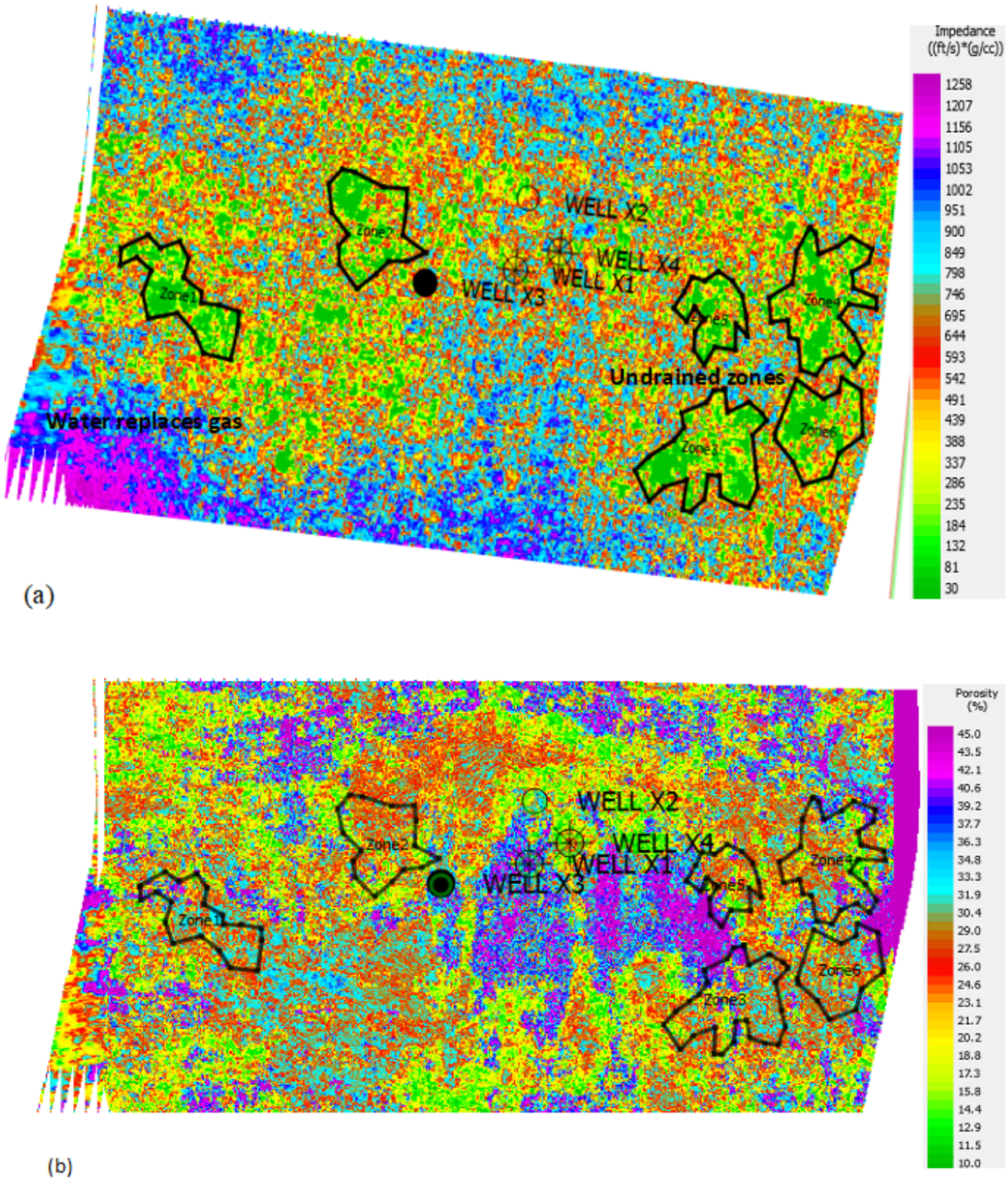

Fig 19. a. Amplitue (Zp) difference map of the bandpass filtered showing delineated bypassed reservoir zones.
b. Porosity estimation slice for bandpass filtered showing high around the delineated bypassed reservoir zones.

6 Conclusion

Bypassed reservoirs saturated with pockets of hydrocarbon accumulation were mapped using full bandwidth and bandpass filtered model-based inversion method. The study demonstrates the need of defining frequency cut-offs for the updated low frequency to size the statistically extracted wavelet from the seismic volume which aids in extracting meaningful 4D P-impedance changes. Six (6) zones have been suspected to show potential to be saturated with bypassed hydrocarbon accumulation. These zones labelled zones 1, 2, 3, 4, 5 and 6 were delineated due to the low impedance usually attributed to hydrocarbon saturated sands, low water saturation and high effective porosity that confirms the connectivity of the zones for hydrocarbon production. From the results of this study, bandpass filter inversion approach showed more reliable and detailed delineated bypassed zones than the full bandwidth approach.

Acknowledgements

We are grateful to Shell Petroleum Development Company (SPDC) of Nigeria Limited, Port Harcourt division for providing datasets used in this study. The authors also appreciate the Hampson Russell Corporation for the software, which enabled us to analyse the data.

References

1) AEO. Annual Energy Outlook. Energy Information Administration United State Department of Energy.. 2018. Available from: https://www.eia.gov/outlooks/aeo/on16/02/2018.
2) Johnston HD, Eastwood EJ, Shyeh JJ, Vauthrin R, Khan M, Stanley RL. Using legacy seismic data in an integrated time-lapse study: Lena Field, Gulf of Mexico. *The Leading Edge*. 2000;19(3):294–302. Available from: https://dx.doi.org/10.1190/1.1438596.
3) Ogbonna-Orji OC, Acra EJ, Adiela UP. Time-lapse Evaluation of Hydrocarbon Production using Rock Properties and Attributes in Niger Delta. *International Journal of Scientific Engineering and Science*. 2017;1:5–10.
4) Landro M, Amundsen L. Introduction to Exploration Geophysics with Recent Advances. Bivrost GeoExPro, Lundin Norway. 2018.
5) Kramers JW. Integrated Reservoir Characterization: from the well to the numerical model. In: and others, editor. 14th World Petroleum Congress. John Wiley and Sons. 1994.
6) Larue DK, Yue Y. How stratigraphy influences oil recovery: A comparative reservoir database study concentrating on deepwater reservoirs. *The Leading Edge*. 2003;22(4):332–339. Available from: https://dx.doi.org/10.1190/1.1572086.
7) Ejedawe J, Love F, Steele D, Ladipo K. Onshore to Deep-water Geologic Integration, Niger Delta. Shell Exploration and Production Limited, Port-Harcourt. Port-Harcourt. 2007.
8) Ajaegwu NE, Odoh BI, Akpunonu EO, Obiadi I, Anakwuba EK. Late Miocene to Early Pliocene Palynosstratigraphy and Palaeo-environments of ANE-1 Well. *Journal of Mining and Geology*. 2012;48:31–43.
9) Weber KJ, Daukoru E. Petroleum Geology of the Niger Delta. *Proceedings of the 9th World Congress*. 1975;2:209–221.
10) Lawrence S, Munday S, Bray R. Regional Geology and Geophysics of the Eastern Gulf of Guinea, Niger Delta to Rio Muni. *The Leading Edge*. 2002;21:1112–1117. Available from: https://doi.org/10.1190/1.1523752.
11) Ehirim CN, Chikezie NO. Anisotropic Avo Analysis for Reservoir Characterization in Derby Field Southeastern Niger Delta. *IOSR Journal of Applied Physics*. 2017;09(01):67–73. Available from: https://dx.doi.org/10.9790/4861-0901016773.
12) Okeugo CG, Onuoha KM, Ekwe CA, Anyiam OA, Dim CIP. Application of crossplot and prestack seismic-based impedance inversion for discrimination of lithofacies and fluid prediction in an old producing field, Eastern Niger Delta Basin. *Journal of Petroleum Exploration and Production Technology*. 2019;9(1):97–110. Available from: https://dx.doi.org/10.1007/s13202-018-0508-6.
13) Doust H, Omatsola E. Niger Delta. In: JD E, PA S, editors. Divergent/Passive Margin Basin;vol. 48. American Association of Petroleum Geologists. 1990;p. 239–248.
14) El-Bahiry M, El-Amir A, Abdelhay M. Reservoir characterization using fluid substitution and inversion methods, offshore West Nile Delta, Egypt. *Egyptian Journal of Petroleum*. 2017;26(2):351–361. Available from: https://dx.doi.org/10.1016/j.ejpe.2016.05.005.
15) Mallick S. Model-based inversion of amplitude-variations-with-offset data using a genetic algorithm. *GEOPHYSICS*. 1995;60(4):939–954. Available from: https://dx.doi.org/10.1190/1.1443860.
16) Castagna JP, Greenberg ML. Shear Wave Velocity Estimation in Porous Rocks. Theoretical Formation, Preliminary Verification and Applications. *Geophysical Prospect*. 1993;p. 195–209. Available from: https://doi.org/10.1016/0148-9062(93)90907-u.
17) Gluyas J, Swarbrick R, Geoscience P. Petroleum Geoscience. and others, editor;Blackwell Science Ltd. 2004.
18) Smith MT, Sondergeld HC, Rai SC. Gassmann fluid substitutions: A tutorial. *Geophysics*. 2003;68(2):430–440. Available from: https://dx.doi.org/10.1190/1.1567211.
19) Archie GE. Classification of Carbonate Reservoir Rocks and Petrophysical Considerations. *AAPG Bulletin*. 1952;36:218–298. Available from: https://dx.doi.org/10.1306/3d9343f7-16b1-11d7-8645000102c1865d.
20) El-Ouair Y, Stronen L. Value Creation from 4D Seismic at the Gulfaks Field: Achievements and Challenges. In: and others, editor. 76th Annual International Meeting, SEG, Expanded Abstracts. 2006;p. 3250–3254. Available from: https://doi.org/10.1190/1.2370206.
21) Oyeyemi DK, Olowokere TM, Aizebeokhai PA. Evaluation of optimal reservoir prospectivity using acoustic-impedance model inversion: A case study of an offshore field, western Niger Delta, Nigeria. *NRIAG Journal of Astronomy and Geophysics*. 2017;6(2):300–310. Available from: https://dx.doi.org/10.1016/j.nrjag.2017.11.001.
22) Rider M. The Geological Interpretation of Well Logs. Blackie, Glasgow. 1986.
23) Landro M, Seismic. Petroleum Geoscience: From Sedimentary Environments to Rock Physics. Bjorlykke K, editor;Springer Science. 2010. Available from: https://doi.org/10.1007/978-3-642-02332-3_19.
24) Johnston D. Practical Applications of Time-lapse Seismic Data: Distinguished Instructor Short Course. Society of Exploration Geophysics, Tulsa, U.S.A. . 2013. Available from: https://doi.org/10.1190/1.9781560803126.
25) Latimer RB, Davidson R, van Riel P. An interpreter's guide to understanding and working with seismic-derived acoustic impedance data. *The Leading Edge*. 2000;19:242–256. Available from: https://dx.doi.org/10.1190/1.1438580.
26) Cemen I, Fuchus J, Coffey B, Gertson R, Hager C. Correlating Porosity with Acoustic Impedance in Sandstone Gas Reservoirs; examples from the Atokan Sandstones of the Arkoma Basin, Southeastern Oklahoma. American Association of Petroleum Geophysics, Annual Convention Exhibition, Pittsburgh, Pennysylvania. Search and Discovery Article #41255. Pittsburgh, Pennysylvania.. 2014.
27) Farvour M, Yoon W, Kim J. Seismic Attributes and Acoustic Impedance in Interpretation of Complex Hydrocarbon Reservoirs. *Journal of Applied Geophysics*. 2015;114:68–80. Available from: https://doi.org/10.1016/j.jappgeo.2015.01.008.